### Title

Air Permeability of Porous Materials Under Controlled Laboratory Conditions




### Journal

Ground Water, 36(4)

### ISSN

0017-467X



### Authors

Springer, David S

Loaiciga, Hugo A

Cullen, Stephen J

et al.



### Publication Date

1998-07-01

### DOI

10.1111/j.1745-6584.1998.tb02829.x

Peer reviewed

# Air Permeability of Porous Materials Under Controlled Laboratory Conditions

by David S. Springer[a], Hugo A. Loaiciga[b], Stephen J. Cullen[c], and Lorne G. Everett[a]

## Abstract

**A series of air permeability tests were conducted on four hand-packed samples of alluvial sands and glass beads using a newly developed air permeameter. The permeameter was tested and found capable of precisely controlling soil-water matric potential (in the range 0 to 1 bar) while simultaneously facilitating the direct measurement of air permeability in porous media. Permeameter results indicate that air permeability increases with a corresponding decrease in water content over a monotonic drainage cycle. It was observed that the rate of change in air permeability with respect to changes in water content is highest at high water content and lowest at low water content. In several soil samples, the air permeability approached a constant value at low water content. Air permeability variations with water content were observed to differ among soils of different texture. For example, the intrinsic permeability of water was 11 to 86% of the maximum air permeability. The new permeameter allowed rapid and accurate measurements of air permeability in fine-textured materials over a wide range of matric potentials and water content.**

## Introduction

Air permeability has been of particular interest to soil and agricultural scientists for decades as it modulates gas exchange between soils and the atmosphere and affects the movement of vadose zone water. Chemical and petroleum engineers have exhaustively investigated the air permeability parameter as it relates to petroleum gas production and migration in oil-field reservoirs. The more recent interest in gas movement in soils as it relates to the migration potential of hazardous, volatile vapors in the subsurface has focused renewed attention on the relations between soil water content and the rate of gas movement through soils. Unsaturated water-air (gas) chemical flow and transport in soils are driven by hydraulic, temperature, and chemical gradients. A complete understanding of such complex multiphase, multispecies flow and transport requires accurate characterization of soil permeability properties with respect to all phases, of which air is fundamental. The objective of this study is to report on (1) the development of an apparatus for the experimental determination of air permeability in soils, referred to as the soil air permeameter with controlled matric potential (SAP-CMP), and (2) the performance of the SAP-CMP in a series of air permeability measurements in artificial porous media and natural soil samples over a wide range of matric potentials and water content.

In this study, the term air permeability, $k_a$ ($L^2$), describes the effective unsaturated permeability to air of a porous medium, where the degree of saturation is determined by the volume fraction of pore space occupied by the air. The term air permeability is thus differentiated from the effective unsaturated permeability to water of a porous medium, $k_w$, in which the degree of saturation is defined by the volume fraction of pore space occupied by water. More importantly, air permeability, as defined in this study, must be clearly differentiated from the intrinsic permeability of a porous medium, k, which depends solely on the properties of the solid matrix and not on the fluid passing through it or the degree of saturation of any fluid phase contained in the pore space (e.g., Bear 1979). It is known from fluid mechanics (Klinkenberg 1941; Scheidegger 1960) that the maximum air permeability (attained when there is no water in the pore space) is larger than the maximum water permeability (attained when the pore space is liquid-saturated) for the same soil sample. Differences in experimentally derived values for the air permeability ($k_a$) and the intrinsic permeability (k) are confirmed as part of the results of this work.

## Brief Overview of Related Work

Klinkenberg (1941) showed that the flow of gases in sintered glass and consolidated sandstone cores under a given pressure field differs from the flow of liquids in that the velocity of gases at the pore wall is generally greater than zero. This phenomenon is called the Klinkenberg effect, and was observed by earlier experimentalists in the late 1800s and coded under the term "slip flow" (Dullien 1992). A consequence of slip flow is that water permeability is generally lower than air permeability in identical porous-media samples. This discrepancy is accentuated at low pressures in fine-textured media and becomes negligible at high pressures in coarse porous media. Other experimental studies conducted from the 1930s through the 1960s (e.g., Wyckoff and Botset 1936; Fancher et al. 1933; Leverett and Lewis 1941; Leas et al. 1950; Gates and Lietz 1950; Yuster 1950; Estes and Fulton 1955; American Petroleum Institute 1952; 1960) supported Klinkenberg (1941) findings.

[a]Geraghty & Miller Inc., 3700 State St., Ste. 350, Santa Barbara, CA 93105.
[b]Department of Geography, University of California, Santa Barbara, CA 93106.
[c]Institute for Coastal Studies, University of California, Santa Barbara, CA 93106-1100.
Received October 1996, accepted October 1997.

Largely based on the methodology and results obtained from earlier studies on rock cores, other air permeability experiments were completed using unconsolidated materials comprising repacked soil core samples (Corey 1957), in situ settings (Kirkham 1946; Grover 1955; Weeks 1978; Davis et al. 1994; Sharp et al. 1994; Hurst and Goggin 1995), and natural and artificial repacked materials (Buehrer 1932; Heid et al. 1950; Stonestrom 1987; Stonestrom and Rubin 1989). Corey (1986) reviewed air permeameter designs. A detailed analysis and comparison of experimental air permeability determinations published in the specialized literature can be found in Springer (1993).

## Methods of Analysis and Results

### Physical Characterization of Test Materials

Two Kern River (Kern County, California) alluvial sediments (repacked, well-graded medium sand and silty sand) and spherical glass beads were used as experimental media during this study. These porous materials were selected for characteristics that rendered them suitable for air permeability testing. Specifically, the materials were free of swelling clays, which permitted a simplification of the design of the rigid-walled permeameter. Also, each of the materials is amenable to artificial repacking. Use of glass beads as an experimental medium was designed to serve as a control material where varying microscale properties that are affected by soil texture, grain shape and packing, and the shape and size of pores can be minimized. The porous materials used in this study were submitted to a series of physical tests following American Society of Testing and Materials (ASTM 1986) standards. Physical parameters that most strongly influence air permeability were determined: particle size distribution (ASTM Standard D422-63), dry bulk density (ρb, procedure described in Springer 1993), porosity (n, procedure described in Springer 1993), soil characteristic curves (using soil moisture pressure plate extractor by Soil Moisture Inc., Santa Barbara, California). In addition, saturated hydraulic conductivity (K, using constant-head permeameter according to ASTM Standard D-2434) and intrinsic permeability (k) were also determined.

Prior to physical characterization, the glass beads were washed with deionized water and oven-dried at 105° F for 48 hours to remove any residue from manufacturing. The natural soil samples were removed from their individual sampling rings, dispersed in deionized water and oven-dried for 48 hours. The packing procedures used for these sample characterization experiments were separated into two steps: (1) mechanical packing within a column (of 1.175 inch ≈ 3 cm diameter); and (2) mass determination of sample plus column to obtain dry bulk density. The first step was facilitated by first adding 1 cm lifts of the homogenized, oven-dried test material into a rigid-walled container of known mass. The first lift was then submitted to a "stabbing" action from a thin and narrow spatula. Stabbing proceeded in a radially outward pattern from the center of the sample and reversing the direction from the margins to the center. Following stabbing, the sample container was dropped a distance of approximately 1 cm for 50 repetitions onto a hard surface (modified after Reeves and Brooks 1953). This dropping and stabbing process was repeated for successive 1 cm lifts until the container was filled to the top. At this stage, the sample/container assembly was weighed and the dry bulk density was calculated. Reproducibility of this method was evaluated by packing glass beads into a cylinder of 15 cm length and 3 cm diameter. Three separate packing trials using the described stabbing/dropping technique showed differences among calculated bulk densities to be less than 0.2% of the mean bulk density.

The test fluid used throughout the physical characterization experiments was a distilled, deionized water with 4 mL of bleach per liter of deionized water. The $HOCL^-$ ion present in the bleach suppressed the growth of microbes and fungi within the test materials during the experiments.

### Results of Physical Characterization of Test Materials

Table 1 contains a summary of selected physical soil parameters and estimates of intrinsic permeabilities (k). Results of sieve analysis for textural properties determination are summarized in Table 1 in terms of $D_{15}$, the grain size for which 15% of the sample particles are finer by weight. All of the test materials are classified as sand, with the natural alluvial materials displaying a greater grain size variation than the glass bead materials.

Saturated hydraulic conductivity values (K) in Table 1 ranged from $7.4 \times 10^{-4}$ cm/s (graded sand EB-2-71.5B) to $1.7 \times 10^{-2}$ cm/s (fine glass beads, GB-A). The intrinsic permeability k ($cm^2$) was determined from the relationship $k = 1.040 \times 10^{-5} K$ (based on the relationship between intrinsic permeability, saturated hydraulic conductivity, water viscosity, and water density, see note 3 in Table 1) with K in cm/s. Bulk dry densities were about the same for all porous-medium samples as shown in Table 1.

Soil water characteristic curves are shown in Figures 1 and 2 for samples GB-A (fine glass beads) and EB-2-71.5 B (sand with silt), respectively. These soil water characteristic curves were generated by means of a pressure plate extractor (see Springer 1993 for details). Soil characteristic curves were determined in order to provide estimates of soil water content in materials during testing based on matric potential. Soil characteristic curves were generated for the test materials in the range of 0 to 15 bars of matric potential (Figures 1 and 2). Figure 1 for the fine glass beads (GB-A) shows a steep slope that develops at about –0.02 bars of matric potential.

**Table 1**
**Summary of Selected Physical Soil Parameters**

| | Sample Designation | | | |
|---|---|---|---|---|
| Parameter | Fine Beads GB-A | Graded Beads GB-B | Graded Sand EB-2-71.5B | Medium Sand EB-9-40 |
| $D_{15}$ (mm)[1] | 0.19 | 0.11 | 0.17 | 0.27 |
| K (cm/s)[2] | $1.7 \times 10^{-2}$ | $7.0 \times 10^{-3}$ | $7.4 \times 10^{-4}$ | $1.3 \times 10^{-2}$ |
| Dry bulk density ($g/cm^3$) | 1.55 | 1.68 | 1.61 | 1.59 |
| Porosity | 0.38 | 0.33 | 0.39 | 0.40 |
| k ($cm^2$)[3] | $1.7 \times 10^{-7}$ | $7.3 \times 10^{-8}$ | $7.7 \times 10^{-9}$ | $1.3 \times 10^{-7}$ |
| $k_{amax}$ ($cm^2$)[4] | $2.31 \times 10^{-7}$ | $8.47 \times 10^{-8}$ | $7.03 \times 10^{-8}$ | $4.01 \times 10^{-7}$ |
| $k/k_{max}$ | 0.74 | 0.86 | 0.11 | 0.32 |
| Air-entry value[5] | 0.32 | 0.27 | 0.32 | 0.33 |
| Field capacity[6] | 0.07 | 0.10 | 0.17 | 0.085 |

[1]Particle size for which 15% of the sample is finer by weight.
[2]K is the unsaturated hydraulic conductivity.
[3]k is the intrinsic permeability estimated from $k = \mu K / \rho g$, where $\mu$ is the viscosity of water ( = 0.0102 g/cm · s), water density $\rho$ = 1 $g/cm^3$, and the average gravity acceleration g = 980 $cm/s^2$, so that $k = 1.040 \times 10^{-5}$ K, where K is in cm/s.
[4]$k_{amax}$ is the maximum measured air permeability, which corresponds to the lowest water contents in Figure 5 through 8.
[5]The air-entry water content as defined in the text.
[6]The water content at which gravitational drainage ceases.

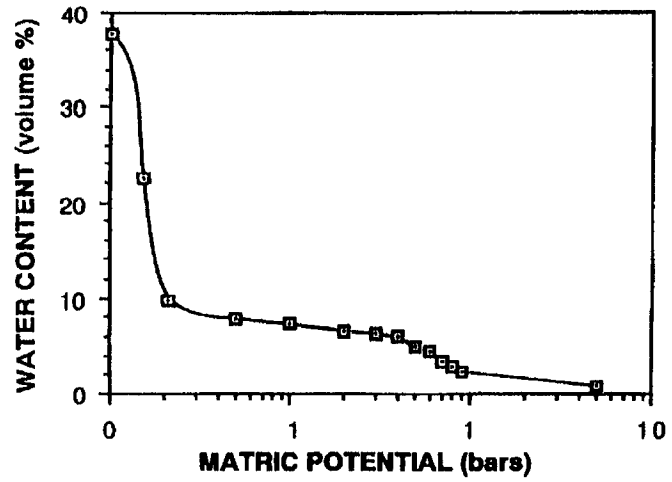


**Figure 1. Soil water characteristic curve for fine glass beads (GB-A).**

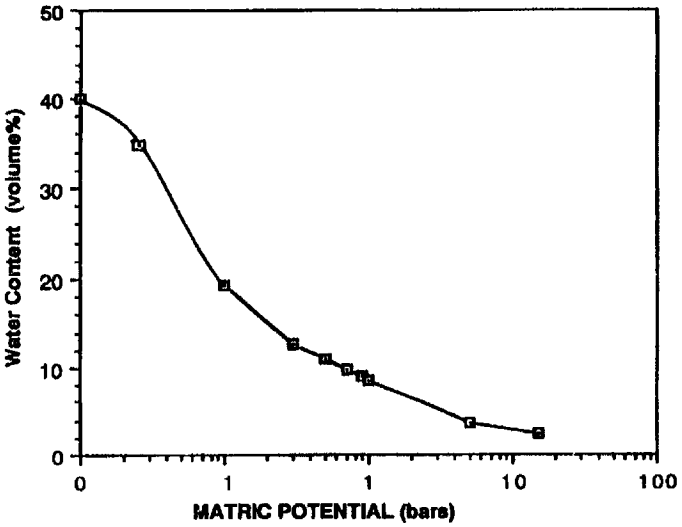


**Figure 2. Soil water characteristic curve for silty sand (EB-2-71.5B).**

This indicates a pronounced drainage from the sample at that matric potential level, which is an indication of the uniformity of the pore radii within the material. Textural analysis of this material confirmed a well-sorted texture. The soil water characteristic curve for the silty sand (EB-2-71.5B) in Figure 2 indicates a much more gradual slope of the water content versus matric potential relationship. This is interpreted to be a direct reflection of the poorly sorted texture of this soil, which is associated with a relatively greater pore radii variation. The behavior of the soil characteristic curves for the two other tested materials, GB-B and EB-9-40, showed the same overall patterns observed in Figures 1 and 2.

## Determination of Air Permeability

A number of assumptions are needed in order to develop an operational air-flow equation for the SAP-CMP apparatus: (1) air permeability can be derived from a modified version of Darcy's law; (2) steady-state flow conditions exist; (3) diffusive air flow within the soil is negligible; (4) isothermal conditions exist in the soil; (5) there is a uniform water content along the axis of flow; (5) there are no macropores or continuous air gaps between the sample and the test cylinder (i.e., wall effects are negligible); (6) gravitational effects contributing to air flow are negligible; (8) moist air behaves approximately as an ideal gas; and (9) slip flow is negligible. Based on these assumptions, the air permeability ($k_a$) can be shown to be a function of the following: the air volume ($Q_0$) flowing through the permeameter's cross section (A); the permeameter's length (L); the dynamic viscosity of air ($\mu$) at ambient temperature; and the air pressures at the inlet ($P_i$) and outlet ($P_0$) of the permeameter, as shown in Equation 1 (see American Petroleum Institute 1952 or Springer 1993 for a derivation of this result):

$$k_a = Q_0 \left\{ \frac{2\mu L}{A} \frac{P_0}{P_i^2 - P_0^2} \right\} \quad (1)$$

Equation 1 is the fundamental (Darcian) expression for air permeability under the assumed conditions. Note that the dynamic viscosity of air is known for a given soil temperature, and all other variables are controllable by experimental design. Therefore, a series of measurements of the air permeability ($k_a$) over a range of volumetric water content provides information as to its behavior as a function of the volumetric water content ($\theta$). This function is herein denoted by $k_a(\theta)$.

Another approach to determining the air permeability from a battery of air-permeameter tests is a graphical one. Equation 1 can be rewritten as:

$$k_a = \frac{A}{B} \quad (2)$$

where $A = Q_0$ and $B = [2\mu\ L / A)\ P_0 / (P_i^2 - P_0^2)]^{-1}$. Under the Darcian flow assumptions, the slope of the best-fit line to a plot of A versus B values at a given water content equals the air permeability for that water content.

## Experimental Apparatus: the Soil-Air Permeameter with Controlled Matric Potential

The SAP-CMP permeameter features tensiometric capabilities which adapt and improve upon the porous plate apparatus used for determination of air permeability (Corey 1957). This new apparatus, referred to as a soil-air permeameter with controlled matric potential (SAP-CMP, patent in application), is a device that precisely controls the soil water matric potential of a cylindrical soil/sediment core in the range of 0 to 100 kPa (0-1 bar). The core of this device is a 1-bar-rated ceramic cylinder which dually acts as a sample holder and as a porous membrane permitting liquid extraction upon the application of suction in the vacuum chamber (Figure 3). The uniform and small pore-size distribution of the ceramic cylinder allows it to remain saturated and hydraulically connected to the soil sample at matric potentials in excess of 100 kPa (1 bar). A ceramic glaze was applied at the ends of the cylinder so that liquid movement can only occur perpendicular to the cylinder walls (radially outward from the soil sample) when suction is applied through the vacuum chamber. These features permit the rapid dewatering of a sample and the establishment of a nearly uniform water content along the axis of flow. After an equilibrium is attained between the matric potential existing within the test sample and the suction in the vacuum chamber, dewatering stops. After equilibrium is attained, the water content in the sample is gravimetrically determined without removing the sample from the ceramic cylinder. This permits a series of tests to be performed at various ranges of water content with minimal physical alteration of the test sample. Rapid sample dewatering and pressure equalization in the permeameter are advan-

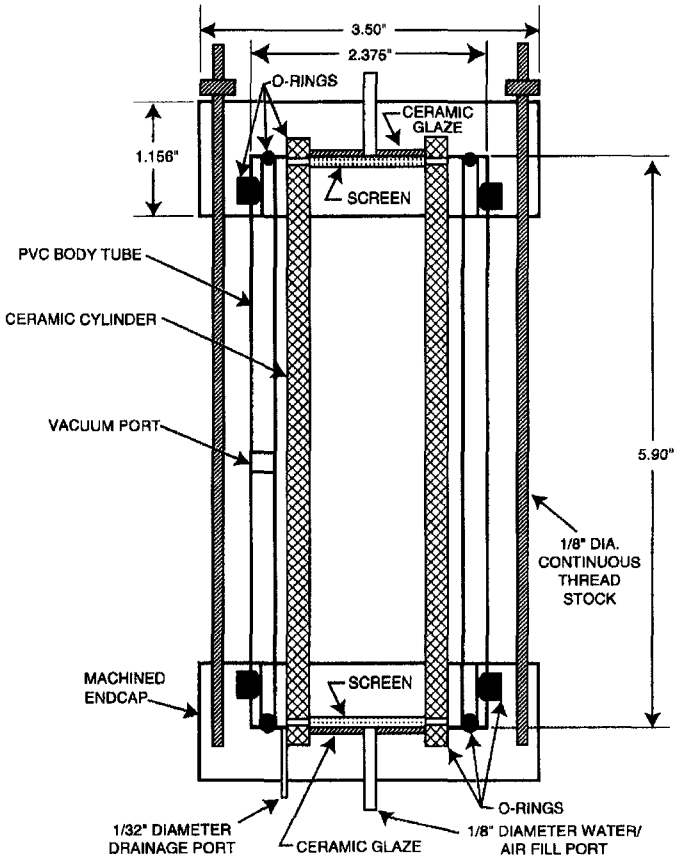


**Figure 3. Detailed cross section diagram of the air permeameter instrument.**

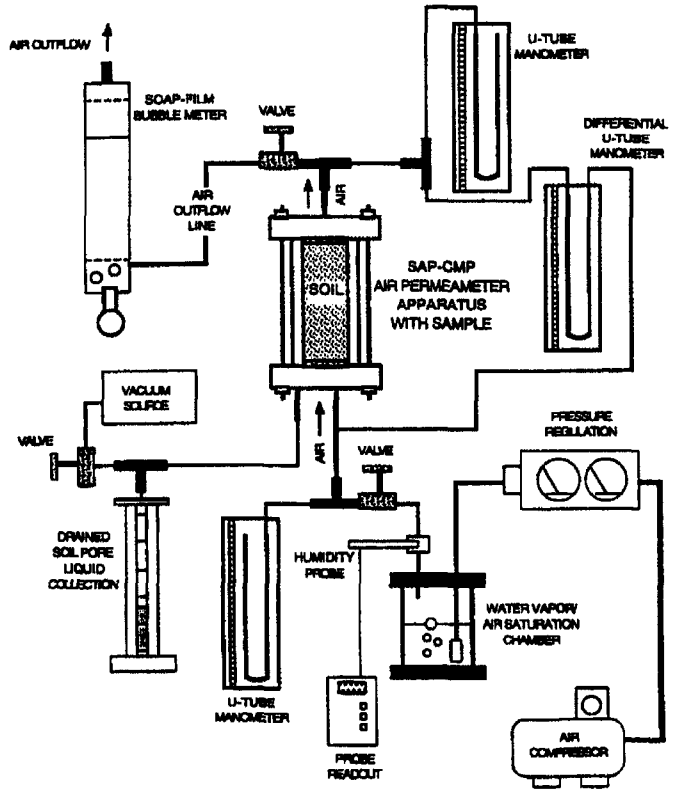


**Figure 4. The soil air permeability permeameter with controlled matric potential instrument.**

tageous features of the SAP-CMP apparatus over earlier air permeameter designs (an early progenitor of our SAP-CMP apparatus is the Hassler permeameter [Hassler 1944], which required complex phase-separating plates and relative long times to equilibrium conditions. See Corey 1986 for a review of air permeameter designs).

A schematic diagram of the air permeability experimental apparatus (SAP-CMP) and its peripheral devices is presented in Figure 4. Starting at the lower right-hand side of Figure 4, pressure is delivered to the inlet of the soil permeameter by means of an air compressor and pressure regulator valve. To avoid drying of the sample by introducing dry air, the injected air is directed into an air water saturation chamber prior to delivery into the permeameter. A relative humidity sensor was mounted at a discharge port of the air water saturation chamber to monitor near-saturation relative humidity in the inlet air stream (pore-air in soils is near saturation with respect to water vapor in most soils). A differential U-tube manometer and two U-tube manometers were installed to measure the air pressure drop $P_i - P_0$ across the permeameter, as well as the individual pressures $P_i$ and $P_0$. (The outlet pressure $P_0$ was equal to atmospheric pressure in this study. However, the experimental setup could easily be modified to establish an outlet pressure other than atmospheric by connecting a pressure regulator to the outlet end of the permeameter.)

The volumetric flow rate of the outlet gas ($Q_0$) was measured using a mechanical flowmeter and a stopwatch. The flowmeter selected for use during this study is a soap film bubble-type meter. It is a highly accurate device that is not affected by the relative humidity of the gas stream or type of gas use in experimentation (see Springer 1993 for details). Because air flow is at steady state when equilibrium conditions hold in the permeameter, the mass (air) flow rate in the flowmeter must be equal to that within the permeameter ($Q_0$). Lastly, water drained from the soil sample in the vacuum chamber was drained to a liquid collection tube (shown in the lower left corner of Figure 4).

## Experimental Procedure and Air Properties

To assess the role of ambient pressure on air flow through the permeameter, barometric pressure fluctuations were monitored at the laboratory site (University of California at Santa Barbara). It was determined that barometric pressure fluctuations at the laboratory site were less than 1 kPa (about 7.51 mm Hg) throughout the experiments. Thus the barometric-corrected pressure term (i.e., B in Equation 2) used in the calculation of the air permeability varied by a maximum of 2%. Given the range of experimental errors that typically arise in the measurement of air permeability, the overall effect of barometric pressure changes during the experiments can be neglected. Air dynamic viscosity ($\mu$) is highly sensitive to temperature and water vapor content. It was determined from thermodynamic equations (Springer 1993) and verified by engineering staff of the American Filter Co. (Kline 1993) that at an ambient temperature of 25° C, and for water vapor saturated air used in the experiments, the dynamic viscosity was equal to 0.0173 centipoise (1 centipoise = 0.01 gr/cm(sec).

An oven-dried, weighed soil sample was introduced into the 3 cm diameter ceramic-walled cylinder as explained previously. Support screen fittings were secured at each end of the ceramic sample holder and the assembly was weighed and recorded. The support fittings were fabricated from screen mesh of adequate size to provide relatively free air flow with minimal pressure losses, while preventing the passage of sample particles. The ceramic cylinder was fitted into the permeameter by securing the top and base acrylic endcaps fitted with O-rings at three positions on each endcap providing an airtight seal.

The soil sample within the ceramic cylinder was connected to a de-aired, distilled water reservoir and slowly vacuum-saturated from bottom to top to minimize the development of air bubbles within the sample. Once saturation was complete, a slight air pressure was applied at the base of the sample to counteract gravitational drainage from the sample. This defined the initial condition (i.e., that corresponding to saturated condition) in the series of air permeability measurements that ensued for increasingly dewatered soil sample conditions. This approach is a modification of the stationary liquid procedure (Osaba et al. 1951; Brooks and Corey 1964).

Starting from saturated conditions, the air pressure at the base of the sample was slowly decreased allowing small increments of water to flow out of the sample. Typically, incremental dewatering continued for a period of three to six days prior to a detectable air permeability. Following each incremental dewatering event, a small air-pressure differential (1 to 2 centibars, 1 centibar = 1 kPa) in excess of the static liquid-pressure differential was initiated and a soap film was created in the outflow bubble meter and continuously monitored in order to evaluate the stage of dewatering where air permeability first became detectable within the sample. At the stage where a distinct and continued movement of the soap film bubble was detected, an air permeability test was performed on the sample by recording volumetric air flow as a function of applied air pressure over a range of pressures and air flows. The measured air pressure and air flow values enabled the calculation of the air permeability, by using Equation 2. The corresponding value of the water content was determined by weighing the sample before and after each air permeability measurement.

Following completion of the first air permeability measurement, continued dewatering was achieved by either permitting continued, controlled, gravitational drainage or by subjecting the test sample to a small vacuum causing pore water within the sample to drain radially outwards through the walls of the ceramic cylinder. During vacuum-assisted drainage, since the entire ceramic sample holder was subjected to a uniform vacuum along the axis of flow, a relatively uniform water content was attained within the test soil. Eventually, the system reached equilibrium, wherein the matric potential within the sample equaled the applied vacuum. At that point visible drainage from the sample ceased. An additional 24-hour period was allowed after visible sample drainage had ceased in order to permit redistribution of pore fluids (air and water) in response to the imposed vacuum. At this point, a permeability test run was completed by applying progressively greater air flow pressure gradients and measuring the resultant air flow rates through the sample. This yielded a set of A and B values, as defined by Equation 2, from which the air permeability was estimated as the slope of the line defined by the plot of the set of A and B values. The water content within the soil sample associated with the estimated air permeability was directly determined by weighing. Further sample dewatering was then implemented to carry out the next estimation of air permeability for the new level of water content. This procedure was repeated for a wide range of water content, thus permitting the devel-

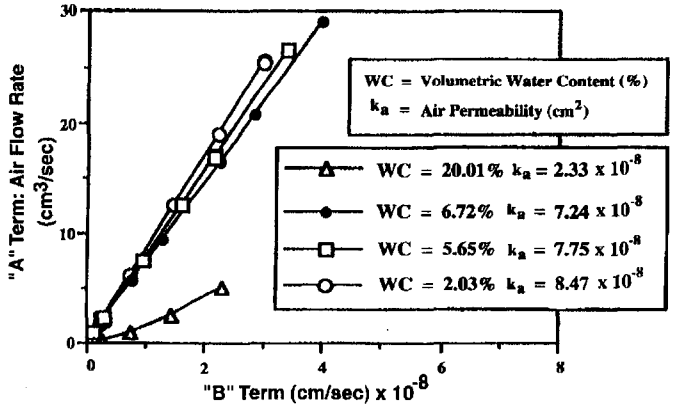


**Figure 5. Graphical air permeability results for glass beads (GB-B). A represents the air flow $Q_0$ and $B = [2\mu L / A) P_0 / (P_i^2 - P_0^2)]^{-1}$, where all terms are defined in Equation 2.**

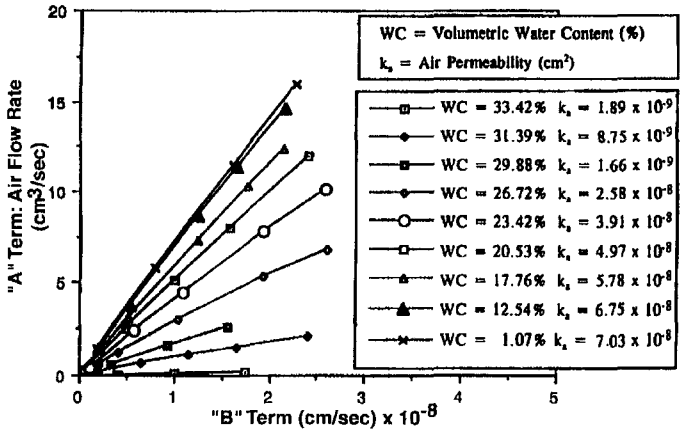


**Figure 6. Graphical air permeability results for silty sand (EB-2-71.5B). A represents the air flow $Q_0$ and $B = [2\mu L / A) P_0 / (P_i^2 - P_0^2)]^{-1}$, where all terms are defined in Equation 2.**

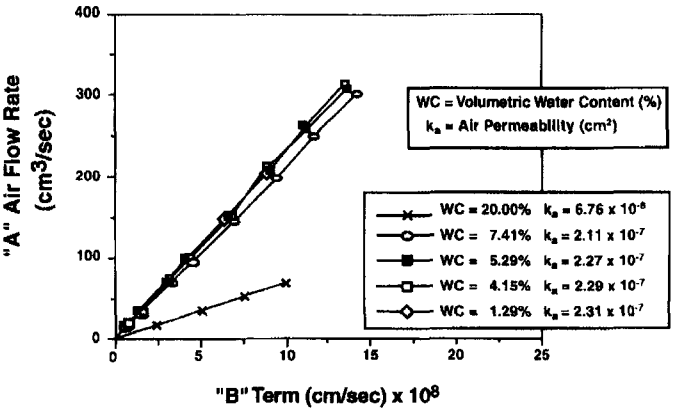


**Figure 7. Graphical air permeability results for glass beads (GB-A). A represents the air flow $Q_0$ and $B = [2\mu L / A) P_0 / (P_i^2 - P_0^2)]^{-1}$, where all terms are defined in Equation 2.**

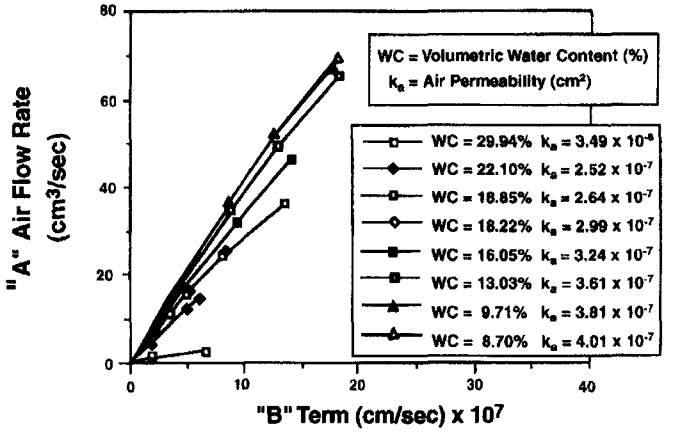


**Figure 8. Graphical air permeability results for sand (EB-9-40). A represents the air flow $Q_0$ and $B = [2\mu L / A) P_0 / (P_i^2 - P_0^2)]^{-1}$, where all terms are defined in Equation 2.**

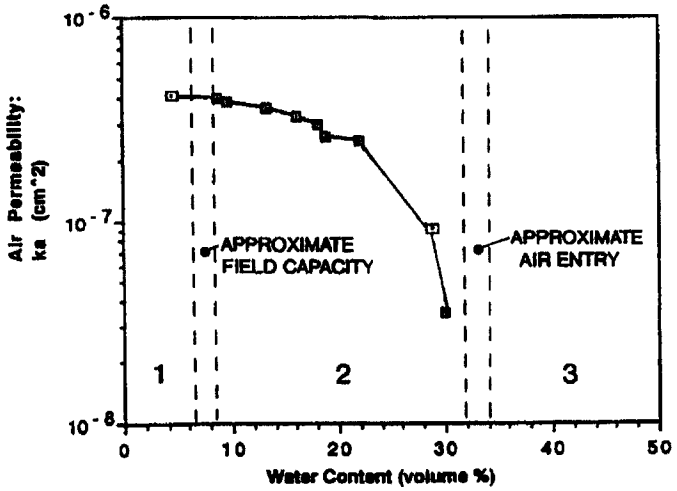


**Figure 9. Air permeability vs. water content for river sand (RB-9-40). The numbers 1, 2, and 3 denote the three regions of air flow behavior described in the text.**

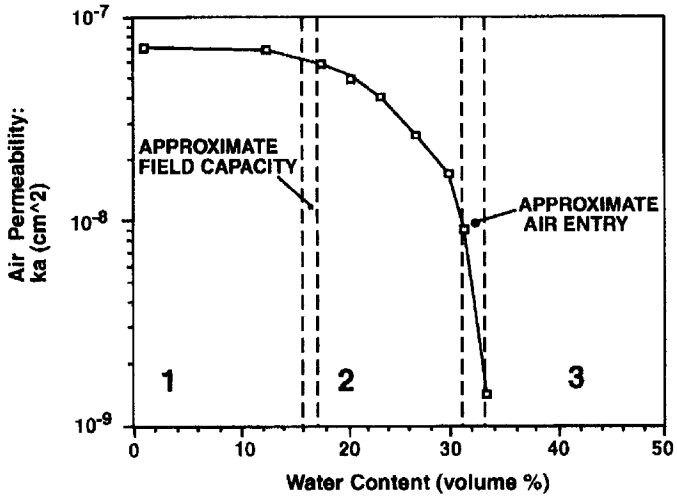


**Figure 10. Air permeability vs. water content for silty sand (EB-2-71.5B). The numbers 1, 2, and 3 denote the three regions of air flow behavior described in the text.**

opment of an air permeability versus water content curve for each soil type, from which the behavior of air permeability as a function of the water content could be ascertained.

### Results of Air Permeameter Testing

Figures 5 and 6 show the plots of A vs. B terms with calculated air permeabilities for the artificial sand GB-B consisting of fine glass beads and for the silty sand EB-2-71.5B, respectively. These two figures illustrate the performance of the SAP-CMP apparatus and the behavior of air permeabilities over a range of water contents in artificial and natural soils. The air permeabilities $k_a$ reported in Figures 5 and 6 are equal to the slopes of best-fit regression lines through the A vs. B data for each water content. Since the best-fit lines nearly intersect the origin of the coordinate axes (i.e., the estimated intercepts from the A vs. B data are close to zero, in agreement with theory according to the definitions of A and B ), it follows that $A = k_a B$ represents the best-fit equation for each water content shown in Figures 5 and 6. The plots in Figure 5 for the fine glass beads, sample GB-B, were derived for four ranges of volumetric water content, ranging from 2.03 to 20.0%. Air permeabilities varied from $8.5 \times 10^{-8}$ cm$^2$ (8.6 Darcies), for a volumetric water content of 2.03% to $2.3 \times 10^{-8}$ cm$^2$ (2.4 Darcies), for a volumetric water content of 20.0%.

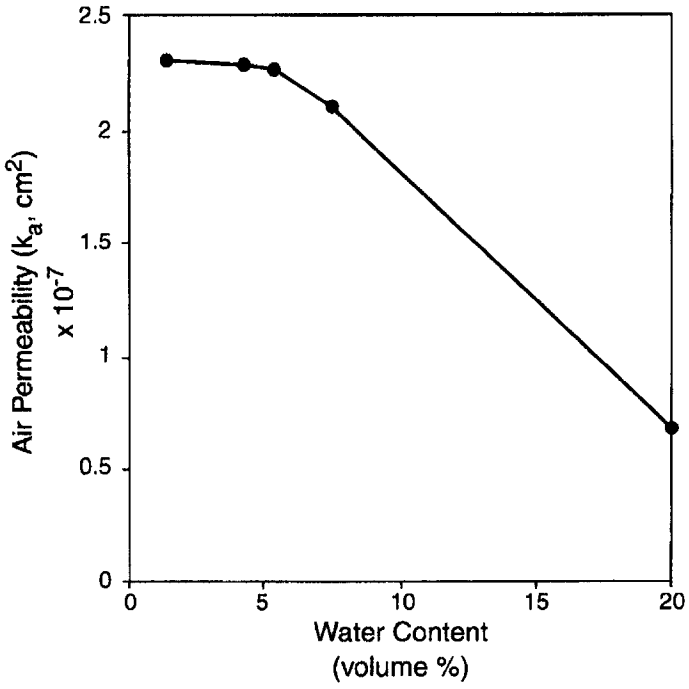


**Figure 11. Air permeability vs. water content for fine glass beads (GB-A). Field capacity and air-entry water contents were estimated at 7% and 32%, respectively (Table 1).**

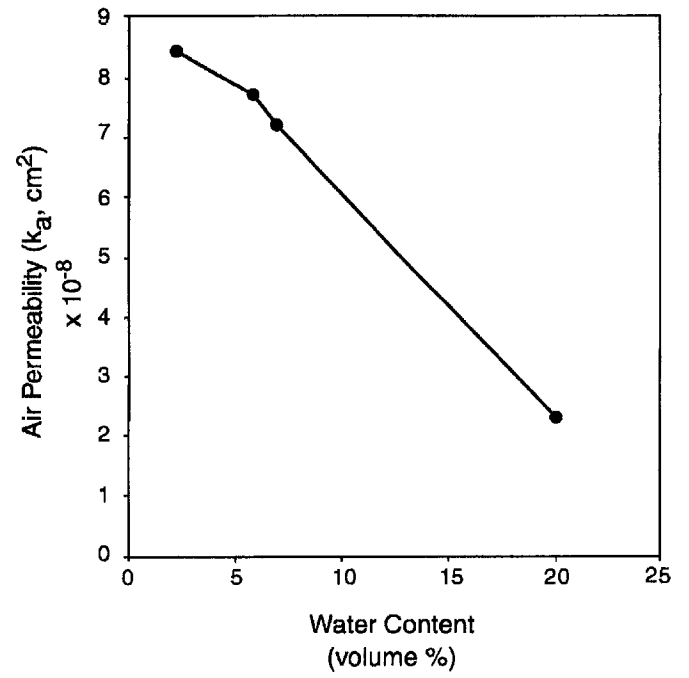


**Figure 12. Air permeability vs. water content for graded glass beads (GB-B). Field capacity and air-entry water contents were estimated at 10% and 27%, respectively (Table 1).**

The A vs. B data points in Figure 5 corresponding to the three lower water contents lie along straight lines which intersect the origin of axes as predicted by the extended Darcian expression (Equation 2). At high water content (20%), the scatter of data increases, causing a slight deviation from a straight line. A tenuous upward curvature is evident for the measurements taken at a volumetric water content of 20%. This is attributed to the high air pressures (in some cases greater that 10 kPa = 10 centibars) that were applied while taking air permeability measurements at relatively high water content: water displacement can occur when the nonwetting

fluid (air) is forced through the test material at a high pressure, while the wetting phase (water) exists as pore liquid occupying and blocking a pore throat. The pressurized air may build up and displace the pore water to a new position resulting in a temporary unsteady-state air flow regime, causing a small departure from the linear relationship between the A and B terms that occurs for strictly steady-state conditions. It is also seen in Figure 5 how the A vs. B curves cluster at progressively lower water contents. This is evidence of convergence to an upper limit of air permeability as air saturation of the pore space is approached, as shown in Figures 7 and 8.

The A vs. B plots in Figure 6, corresponding to the silty sand (sample EB-2-71.5B), encompass a wide range of nine water contents, varying from air-dry to near saturated conditions. In this case, the linearity of the derived curves, all of which nearly intersect the origin (within the precision allowed by experimental error), indicate an correspondence with the theoretical model. This correspondence was observed even at relatively high water content which required the application of higher air pressure gradients. Figure 6 shows the clustering and convergence of the air permeabilities to an upper limit as air saturation of the pore space is approached. Slope-determined $k_a$ values ranged from $7.03 \times 10^{-8}$ $cm^2$ to $1.89 \times 10^{-9}$ $cm^2$ for corresponding increases in volumetric water content from 1.07 to 33.4%, respectively.

Figures 7 and 8 show the A vs. B data with calculated air permeabilities for several levels of water content for the glass beads GB-A and sand EB-9-40, respectively. The patterns of the data shown in Figures 7 and 8 are similar to those shown in Figures 5 and 6, respectively, although a slight downward curvature occurred for the measurements taken at water contents of 13.0%, 16.0%, and 18.9% in Figure 8. This is attributed to accidental errors (i.e., introduced by chance) that occurred in testing sample EB-9-40, rather than to systematic errors.

Figures 9 and 10 display plots of air permeability ($k_a$) versus volumetric water content ($\theta$) for the two river sand samples EB-9-40 and EB-2-71.5B, respectively. The results associated with these two samples capture the overall behavior of air permeability as function of water content determined with the SAP-CMP instrument. It is clear from these figures the existence of upper and lower limits for air permeability as the water content approaches either negligible values or the porosity of the material, respectively.

The relationship between water content and air permeability is separated into regions 1, 2, and 3 in Figures 9 and 10. Region 3 encompasses the soil water condition, which extends from saturation to "air entry." Since air permeability theoretically emerges at the air entry value, this region is characterized by the inception of air permeability, and thus the lowest magnitude of air permeability measured within a porous material. The water content corresponding to air entry was determined to vary between 27 and 33% for the tested samples (Table 1). These air-entry values fluctuate between 80 to 85% of the porosity of each test sample, in agreement with experimental evidence provided by Corey 1986. For water content in excess of the air-entry water content, no air-filled continuous conduit exists, thus precluding the existence of air permeability.

Region 2 (Figures 9 and 10) lies in the water content range from air entry to the estimated field capacity of each test material. The field capacity of a soil is that level of water content at which gravitational drainage within the soil ceases. It is determined experimentally in a soil column by determining the equilibrium water content at which gravitational drainage ceases following dewatering from saturated conditions. In this study, field capacity (water content) was achieved after 48 hours of gravitational drainage. Figures 9 and 10 show that region 2 is characterized by the most significant changes in air permeability. Progressive dewatering of a porous material from an initially saturated state will proceed in the order of the largest pore draining first, in accordance with capillary theory. At the emergence of air permeability, few interconnected pores may exist with which to transmit air. As drainage proceeds from air entry, the network of interconnected, dewatered pores increases while opening up progressively smaller-diameter pores. The air permeability increases abruptly as the water content falls slightly below the estimated air-entry water content. As drainage continued toward and beyond the approximate field capacity in these sandy materials, the air permeability is seen to approach an upper limit. Lastly, region 1 in Figures 9 and 10 corresponds to the soil water condition that exists in a test sample from field capacity to dry conditions. The magnitude of the air permeability in region 1 is shown to be at or near its maximum measured value. The field capacity values shown in Figures 9 and 10 are reported in Table 1.

Figures 11 and 12 display the $k_a$ vs. $\theta$ figures for the glass beads GB-A and GB-B, respectively. Figure 11 for medium GB-A shows a variation of air permeability with water content similar to those observed for the river sands shown in Figures 9 and 10. Because of the glass beads' unique texture, the air permeability could not be determined accurately with water content exceeding 20% due to fluid displacement caused by injected air. The variation of air permeability with water content in medium GB-B, shown in Figure 12, displays an almost linear relationship between air permeability and water content in the range of water content from about 7 to 25%. The air permeability curve flattens off below a water content of 7%. Air-entry and field capacity values for the glass beads GB-A and GB-B are shown in Table 1.

## Summary and Conclusions

The main objective of this study was to report on a newly developed SAP-CMP permeameter and its performance on a series of laboratory measurements of air permeability. The application of the permeameter to air permeability measurements in natural and synthetic porous media samples confirmed previous experimental results on air permeability variations with water content. It also revealed new information on the variability of air-transmissive properties of soils with different textures. The main conclusions of this study are as follows:

1. The specialized air permeameter (SAP-CMP) instrument developed and constructed as part of this study performed well within its design functions. The SAP-CMP apparatus achieved rapid and precise axial dewatering and simultaneous air permeability measurements of test materials with minimum physical alteration during experimentation, except at high water contents when larger air pressures were required to overcome pore water displacement.
2. Results obtained from graphical analysis of the experimental data are consistent with the Darcian model equation in describing steady-state, vertical, single-phase, isothermal, compressible gaseous flow through porous media for a wide range of applied differential air pressures. Slight deviations from Darcian air flow were observed only at very high applied differential

air pressures due to probable pore water displacement, confirming the robustness of Darcy's law (Equation 2) for describing air flow.

3. The behavior of the air permeability function with a monotonically decreasing water content in test materials EB-9-40 (medium river sand) and EB-2-71.5B (medium river sand with 7% silt) indicates a progressive increase in air permeability with a corresponding decrease in the volumetric water content. The rate of change in air permeability with respect to changes in water content was lowest below field capacity and largest near the water content range approaching the air-entry water content. All tested samples showed a convergence to an upper limit in air permeability as water content was reduced to near zero levels.
4. The ratio of intrinsic permeability (defined with respect to water movement) to maximum air permeability calculated for the four types of porous media varied between 0.11 to 0.86, demonstrating the variability of air-transmissive properties as a function of soil texture.

One promising research area on air permeability would be to extend the types of experimental measurements conducted in this work to a broader range of soils and develop mathematical relations of air permeability as a function of soil water content. Although work of this kind has been done for unsaturated water conductivity (e.g., Van Genuchten 1980), the mathematical characterization of air permeability remains a fruitful area of research.

## Acknowledgments

This research was supported in part by the U.S. Environmental Protection Agency Cooperative Agreement CR-816969-01-0, and grants 94-09 and NSF-SES-88-109-17 from the Kearney Foundation of Soil Science and the National Science Foundation, respectively. Three anonymous reviewers contributed to the improvement of this article.

## References

American Petroleum Institute. 1960. *Recommended Practice for Core Analysis Procedure.* A.P.I. R.P. 40, Dallas, Texas.

American Petroleum Institute. 1952. *Recommended Practice for Determining Permeability of Porous Media.* API RP 27, 3rd. ed. Dallas, Texas.

American Society of Testing and Materials. 1986. *Methods of Soil Analysis.* New York.

Bear, J. 1979. *Hydraulics of Groundwater.* New York: McGraw-Hill.

Brooks, R.H., and A.T. Corey. 1964. *Hydraulic Properties of Porous Media.* Hydrology Paper No. 3, Colorado State University, Fort Collins, Colarado.

Buehrer, T.F. 1932. *The Movement of Gases Through Soil as a Criterion of Soil Structure.* Arizona Agricultural Station Technical Bulletin 39.

Corey, A.T., 1957. Measurement of water and air permeability in unsaturated soils. *Soil Science Society of America Procs.* 21, 7–10.

Corey, A.T. 1986. Air Permeability, Methods of Soil Analysis, Part 1. In *Physical and Mineralogical Methods*, 2nd ed., ed. A. Klute, Number 9 in the Series Agronomy, 1121–1136. Madison, Wisconsin: American Society of Agronomy, Soil Science Society of America.

Davis, J.M., J.L. Wilson, and F. Phillips. 1994. Ground water, a portable air minipermeameter for rapid in situ field measurements. *Ground Water* 32, no. 2: 258–266.

Dullien, A.F.L., 1992. *Porous Media*, 2nd. ed. San Diego: Academic Press.

Estes, R.K., and P.F. Fulton. 1955. Gas slippage and permeability measurements. *Transactions American Institute of Mechanical Engineers* 207, 338–342.

Fancher, G.H., J.A. Lewis, and K.B. Barnes. 1933. *Some Physical Characteristics of Oil Sands.* Experimental Station Bulletin 12. Penn. State College of Mineral Industries.

Gates, J.I., and T. Liet. 1950. Relative permeabilities of California cores by the capillary-pressure method. *American Petroleum Institute of Drilling and Production Practice* 285–297. New York: API.

Grover, B. L. 1955. Simplified air permeameters for soils in place. *Soil Science Society of America Procs.* 19, 414–418.

Hassler, G. 1944. *Method and Apparatus for Permeability Measurements.* U.S. Patent Number 2,345,935. Washington, D.C.: U.S. Patent Office.

Heid, J.G., J.J. McMahon, R.F. Nielsen, and S.T. Yuster. 1950. Study of the permeability of rocks to homogeneous fluids. *Drilling and Production Practice* 230–244. New York: API.

Hurst, A. and D.J. Goggin. 1995. Probe permeametry: An overview and bibliography. *AAPG Bulletin* 79, no. 3: 463–473.

Kirkham, D. 1946. Field methods for determination of air permeability of soil in its unsaturated state. *Soil Science Society of America Procs.* 11, 93–99.

Kline, R. 1993. Interview by author, September 11, Santa Barbara, California.

Klinkenberg, L.J. 1941. The permeability of porous media to liquids and gases. *American Petroleum Institute Drilling and Production Practice* 200–213.

Leas, W J., L.H. Jenks, and C.D. Russell. 1950. Relative permeability to gas. *Transactions of the American Institute of Mechanical Engineers* 189, 65–72.

Leverett, M.C., and W.B. Lewis. 1941. Steady flow of gas-oil-water mixtures through unconsolidated sands. *Transactions of the American Institute of Mechanical Engineers* 142, 107–116.

Osaba, J.S., G. Richardson, J.K. Kerver, J.A. Hanford, and P.M. Blair. 1951. Laboratory measurements of relative permeability. *Transactions of the American Institute of Mechanical Engineers* 192, 47–56.

Reeves, R.C., and R.H. Brooks. 1953. Equipment for subsampling and packing fragmented soil samples for air and water permeability tests. *Soil Science of America Proceedings* 17, 333–336.

Scheidegger, A.E. 1960. *The Physics of Flow Through Porous Media*, 2nd. ed. Toronto: University of Toronto Press.

Sharp, J.M. Jr., L. Fu, P. Cortez, and E. Wheeler. 1994. An electronic minipermeameter for use in the field and laboratory. *Ground Water* 32, no. 1: 41–46.

Springer, D.S. 1993. Determining the air permeability of porous materials as a function of a variable water content under controlled laboratory conditions. M.A. thesis, Dept. of Geography, University of California, Santa Barbara, California.

Stonestrom, D.A. 1987. Co-determination and comparisons of hysteresis-affected parametric functions of unsaturated flow: Water content dependence on matric pressure, air trapping, and fluid permeabilities in a non-swelling soil. Ph.D. diss., Applied Earth Petroleum Engineering, Civil Engineering, Stanford University, Stanford, California.

Stonestrom, D.A., and J. Rubin. 1980. Air permeability and trapped-air content in two soils. *Water Resources Research* 25, no. 9: 1959–1969.

Van Genuchten, M.Th. 1980. A closed-form equation for predicting the hydraulic conductivity of unsaturated soils. *Soil Science Society of America Journal* 44, 892–898.

Weeks, E.P. 1978. Field determination of vertical permeability to air in the unsaturated zone. U.S. Geological Survey Paper 1051. Washington, D.C.: U.S. Government Printing Office.

Wyckoff, R.D., and H.G. Botset. 1936. The flow of gas-liquid mixtures through unconsolidated sands. *Physics* 7, 325–345.

Yuster, S.T. 1950. Homogeneous permeability determination. *Drilling and Production Practice* 356–363. New York: API.